

Crucial effect of glass processing and melt homogenization on the fragility of non-stoichiometric chalcogenides

Sriram Ravindren¹, K. Gunasekera¹, Z. Tucker¹, A. Diebold², P. Boolchand¹, M. Micoulaut³

¹*School of Electronics and Computing Systems, College of Engineering and Applied Science, University of Cincinnati Cincinnati, OH 45221-0030, USA*

²*Department of Physics, University of Cincinnati, Cincinnati, OH 45221-0011, USA and*

³*Laboratoire de Physique Théorique de la Matière Condensée, Université Pierre et Marie Curie, 4 Place Jussieu, F-75252 Paris Cedex 05, France*

(Dated: January 15, 2021)

The kinetics of homogenization of binary $\text{As}_x\text{Se}_{100-x}$ melts in the As concentration range $0\% < x < 50\%$ are followed in FT-Raman profiling experiments, and show that 2 gram sized melts in the middle concentration range $20\% < x < 30\%$ take nearly two weeks to homogenize when starting materials are reacted at 700°C . In glasses of proven homogeneity, we find molar volumes to vary non-monotonically with composition, and the fragility index \mathcal{M} displays a broad global minimum in the $20\% < x < 30\%$ range of x wherein $\mathcal{M} < 20$. We show that properly homogenized samples have a lower measured fragility when compared to larger under-reacted melts. The enthalpy of relaxation at T_g , $\Delta H_{nr}(x)$ shows a minimum in the $27\% < x < 37\%$ range. The super-strong nature of melt compositions in the $20\% < x < 30\%$ range suppresses melt diffusion at high temperatures leading to the slow kinetics of melt homogenization.

PACS numbers: 61.43.Fs

I. INTRODUCTION

Fragility of glass forming melt historically emerged from investigations of the temperature dependence of viscosity¹. The manner in which viscosity (η) of such melts increases as melts are cooled to the glass transition temperature T_g can be used to characterize viscous slow down of supercooled liquids. Since η is proportional to a shear relaxation time τ through the Maxwell relation ($\eta = G_\infty \tau$) where G_∞ is the bulk modulus at infinite frequency, it is convenient to define the fragility \mathcal{M} index as

$$\mathcal{M} \equiv \left[\frac{d \log_{10} \tau}{dT_g/T} \right]_{T=T_g} \quad (1)$$

The dimensionless slope \mathcal{M} , examined in a wide variety of glass forming liquids², is found to vary between a high value³ of 214 to a low value⁴ of 14.8. Melts possessing a high value are termed as "fragile" while the ones with a low value are "strong". Fragile melts usually show a highly non-exponential variation of $\eta(T)$ while strong ones have a nearly Arrhenius variation². At high T , both variations lead to the same value of η ⁵. The non-exponentiality of η in glass forming melts has been fitted in terms of various functions such as Vogel-Fulcher-Tamman (VFT⁶) given by:

$$\eta = \eta_0 \exp \left[\frac{A}{T - T_0} \right] \quad (2)$$

where A and T_0 are fitting parameters, or the Mauro-Yue-Ellison-Gupta-Allan (MYEGA⁷) or Avramov-Milchev (AM⁸) functional forms.

Since the inception of the strong-fragile melt classification, $\eta(T)$ variation in stoichiometric glass forming melts such as the oxides, chalcogenides, alcohols, sugars, and organic polymers has been well documented⁹ in a plot initially introduced by Laughlin and Uhlmann¹⁰, and subsequently popularized

by Angell¹¹. The case of non-stoichiometric inorganic glass forming melts has been explored much less. In an early study on the As-Ge-Se ternary¹² it was recognized that the fragility index of such alloyed melts shows a minimum near a mean coordination number $\bar{r} = 2.40$, identified with the location of a mean-field flexible to rigid transition^{13,14}. More recent work on the $\text{Ge}_x\text{Se}_{100-x}$ binary has shown⁴ that the fragility index \mathcal{M} takes on a rather low value of 14.8(5) near a Ge concentration of $x = 22\%$ corresponding to a mean coordination number $\bar{r} = 2.44$ residing in the Intermediate Phase of corresponding bulk glasses¹⁵⁻¹⁷ where the enthalpic relaxation at the glass transition temperature is minuscule. A theoretical link between enthalpic changes, fragility and isostatic character of the glass network has been established from a simple Keating model reproducing the behavior of covalent glass-forming liquids¹⁸.

The observation of important fragility minima (i.e. super-strong melts) has actually profound consequences. The super-strong character over selected compositional ranges has, in fact, deep implications on the homogenization of corresponding melts. This is the case because melt viscosity for such compositions at high temperatures, where melts are equilibrated, far exceed those of the more fragile compositions outside of this compositional window. The wide variations in melt viscosity with composition thus leads -in a natural fashion- to hindered diffusion which is manifested as a slow batch homogenization^{19,20}.

In this work we show, for the first time to the best of our knowledge, that $\text{As}_x\text{Se}_{100-x}$ melts in the $20\% < x < 35\%$ composition range are quite strong with a very low fragility index $\mathcal{M} < 20$, and the lowest one being found for the $x=24\%$ composition, which corresponds to a fragility index of $\mathcal{M}=16.4$, i.e. slightly less than that of silica, which is traditionally thought of as the archetypical strong liquid²¹⁻²³. Melt compositions outside this broad compositional window possess higher fragility indices. This leads amongst other things

to the dynamics of melt homogenization during glass melting to qualitatively slow down. Melt homogenization is a critical subject that is, unfortunately, often overlooked in the literature. Here we bring a quantitative connection between fragility measurements and the ease of homogenization. Several broad consequences emerge. One, these conditions, as in the case of the Ge-Se binary⁴, also cause As-Se melts to undergo slow homogenization as we demonstrate here directly from FT-Raman profiling experiments. Second, the broad fragility window residing in the mean-coordination number range of $2.20 < \bar{r} < 2.35$, correlates more or less with a minimum in the enthalpy of relaxation at T_g in corresponding glasses (reversibility window²⁴), and both are shifted to $\bar{r} < 2.40$. Third, because of slow homogenization of As-Se melts, physical properties of these melts/glasses are notoriously non-reproducible^{25,26}. We highlight this important issue for molar volumes and fragility index measurements in this context. Previous conclusions drawn for Ge-Se are fully recovered⁴ and underscore the generality of the above statements.

The paper is organized as follows. After presenting the experimental results in section II, and the method of Raman profiling which allows to check for the homogeneity of the samples, we present the experimental results on fragility activation energy for relaxation and molar volume in section III. We discuss the consequences of the findings in section IV, and show that general correlations can be drawn. Finally, the conclusions are summarized in section V.

II. EXPERIMENTAL

A. Synthesis of glasses

Bulk glasses of the $\text{As}_x\text{Se}_{100-x}$ binary were synthesized using elemental Se (5N purity, 3-4 mm dia., Cerac Inc.), and As_2Se_3 (5N purity, 1-6 mm granules, Noah Technologies) as precursors. As-rich glasses ($x > 40\%$) made use of As_2Se_3 and $\text{As}_{50}\text{Se}_{50}$; the latter synthesized using pure As (5N purity, large lumps, Cerac Inc.) and As_2Se_3 precursors. Prior to their use, the clean ampoules were dried in a vacuum oven at 90°C for 24 hours. The ingredients were mixed in the desired ratio by weight to give a total of 2 grams (to an accuracy of 0.1 mg) per sample and subsequently batched in quartz tubing (5 mm ID, 7 mm OD). The precursors were not crushed in order to keep to a minimum the surface area available to oxidation and water adsorption. It is unclear if As-Se melt homogenization is significantly accelerated by crushing the precursors; factors such as viscosity overwhelmingly determine the homogenization period. The mostly nodular precursors served to facilitate attainment of high vacuum ($\approx 3 \times 10^{-7}$ Torr) using a liquid N_2 -trapped high vacuum pumping system, and the quartz tubes sealed using a Hydrogen-Oxygen torch. Typical ampoule length was between 75-90 mm. The sealed ampoules, positioned vertically in a T-programmable vertical tube furnace, were reacted by initially ramping T up linearly from 25°C to 700°C over 13 hours, and then held at 700°C until melts homogenized for periods lasting up to two weeks

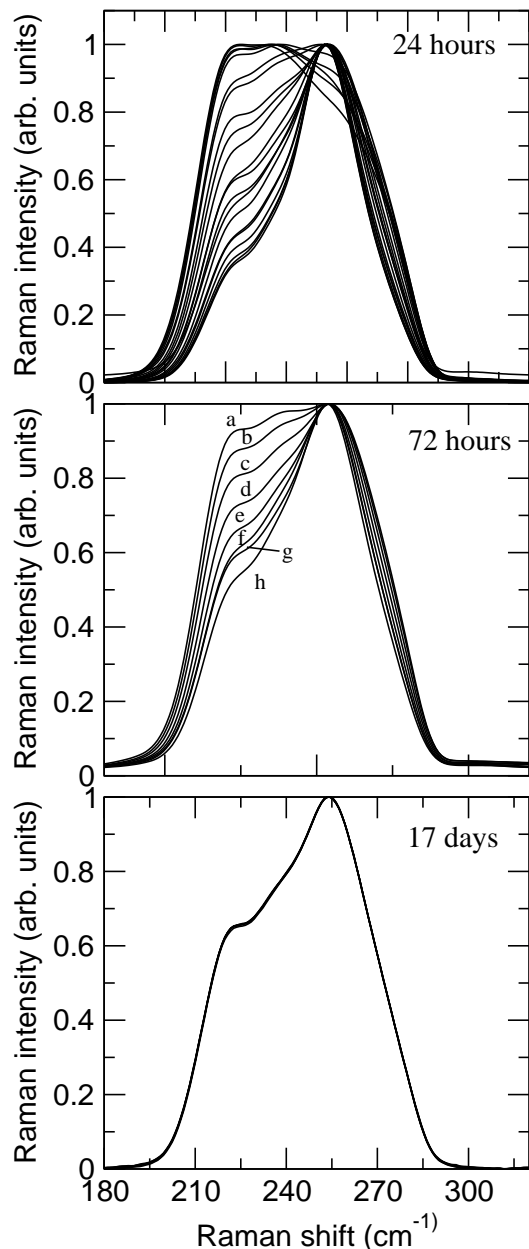


Figure 1: FT Raman profiling of a $\text{As}_x\text{Se}_{100-x}$ melts at $x = 24\%$ taken after indicated reaction times T_R (24 hours, 72 hours and 17 days). Melts are heterogeneous at $T_R < 24$ hours, but steadily homogenize as the reaction time increases to several days. We show that the underlying factor is the fragility of melts.

in some cases. Prior to removing the samples from the furnace, the temperature was lowered to 50°C above the reported liquidus^{27,28} and equilibrated at that T for 2 hours, prior to a water quench.

Melts were periodically FT-Raman profiled (see below) to map the diminishing heterogeneity. Once melt homogeneity was established, these were T_g -cycled *in situ* by holding isothermally at $T_g(x)+20^\circ\text{C}$ for 30 minutes (to remove residual stresses) in a box furnace, and slow cooled at $3^\circ\text{C}/\text{min}$ to room temperature to realize homogeneous bulk glasses.

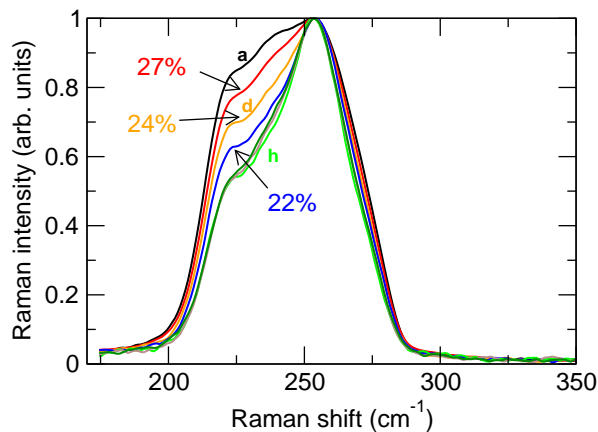


Figure 2: Fractionation of the $\text{As}_{24}\text{Se}_{76}$ melt reacted at 700°C for 3 days is revealed in this stacked Raman spectra. Some of the observed lineshapes are characteristic of specific compositions. This plot illustrates the extent to which the melt resists homogeneity with a spread of nearly 7%.

Glasses were then removed from evacuated quartz tubes, and weighed for Modulated-DSC (≈ 20 mg), Fragility (≈ 10 mg) and Molar volume (>200 mg) measurements.

B. Raman line profiling of quenched melts

Melt homogeneity was ascertained using an FT-Raman spectroscopic line profiling method^{19,20}. Raman vibrational density of states (VDOS) of $\text{As}_x\text{Se}_{100-x}$ glasses vary measurably with glass compositions ‘ x ’. Melt heterogeneity was tracked by recording FT-Raman spectra along the length of the melt column encased in quartz tubing, first after 72 hours of reaction, and then every 48 hours thereafter until all lineshapes recorded along the melt column became identical when they were considered to be fully homogeneous. We used a Thermo Nicolet NXR FT-Raman module with 1064 nm (1.17 eV) radiation from an Nd-YAG laser to excite the scattering. The laser spot size was at $50 \mu\text{m}$. A typical measurement at a single location involved 100 scans at 2 cm^{-1} resolution (219.70 seconds/location) using a laser power of 105 mWatts.

Raman spectral acquisition was programmed for typically 8 equidistant sample-focused points along the length of the quartz tube. These spectra were baseline adjusted, amplitude corrected and stacked to qualify spectral overlap. The uniqueness of a composition’s spectral signature implies that complete spectral overlap is critical to establishing sample homogeneity. Observable differences in stacked lineshapes suggest variations in local sample stoichiometry ‘ x ’, implying heterogeneity of the reacted batch composition. After full homogenization was established, a library of high resolution Raman spectra was acquired at each composition in the $0\% < x < 50\%$ range. The library provided a basis to track the evolution of homogeneity over time.

Fig. 1 illustrates an example of a Raman profiled result. The three panels provide a global view of melt homogenization kinetics at $x = 24\%$. It is observed that all 8 Raman line-

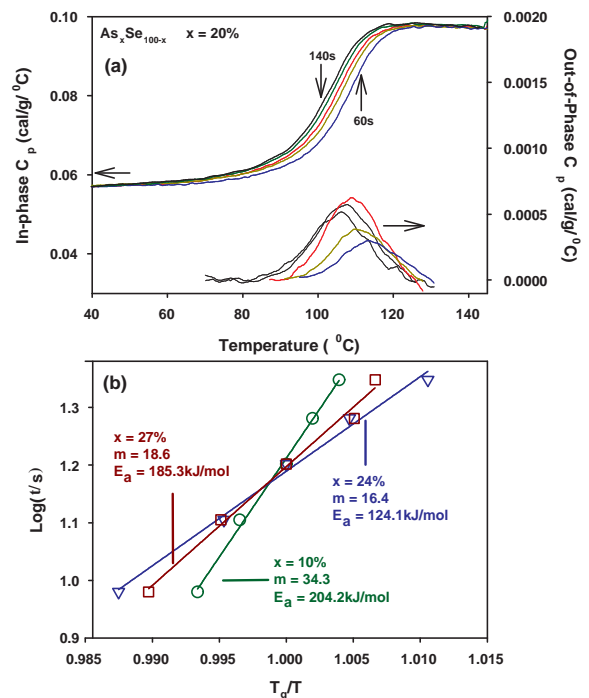


Figure 3: The real (a) and imaginary (b) parts of the complex heat capacity C_p^* for an $\text{As}_{20}\text{Se}_{80}$ glass were obtained from MDSC measurements at a rate of $3^\circ\text{C}/\text{min}$ and a modulation amplitude of 1°C over five periods ($1^\circ\text{C}/60\text{s}$, 80s , 100s , 120s , 140s). The fragility index was extracted from the slope of the curves at $T_g/T=1$ in the Angell plot.

shapes taken along the melt column coalesce after heating at 700°C for 17 days. From such studies we were able to generate a library of Raman spectra of homogenized melts at 20 compositions in the range $0\% < x < 50\%$, and it is used in analyzing the profiled Raman spectra given that important information on the nature of structural heterogeneity across a melt column is contained in the observed spread of Raman line-shapes as highlighted by profiling results of a melt at $x = 24\%$ after being reacted at 700°C for 3 days (Fig. 2). It is seen that three of the observed line-shapes in that group of 8 correspond exactly to melt stoichiometry of $x = 22\%$, 24% and 27% as indicated in Fig. 2. These data show that the As content along the length column exhibits a gradient; it has a maximum value of about $x = 28\%$ at the bottom and a minimum value of $x = 21\%$ at the top of the melt column. Thus, we find that for the 2 gram sized melt, reacted at 700°C for 3 days, the As stoichiometry varies by nearly 7% across the melt column, and would inevitably lead to some spread if a physical measurements were to be undertaken from glasses having been prepared at this reaction time.

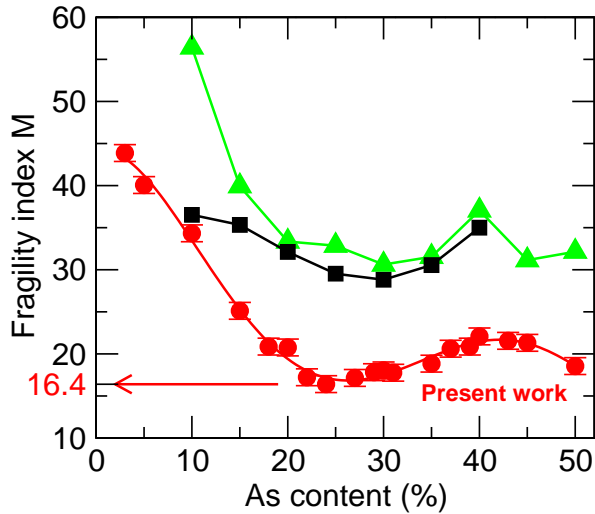


Figure 4: Compositional variation of the fragility index \mathcal{M} of the As-Se system as reported in present work (●), compared with other recent reports (■, Ref. 25; ▲, Ref. 26).

III. RESULTS

A. Fragility measurements

Melt fragility were established by recording the complex C_p heat flow (C_p^{real} , $C_p^{imaginary}$) near T_g using a TA Instruments Q2000 MDSC system. A 10 mg quantity of a glass sample sealed in an aluminum pan, was cooled starting from $T_g+50^\circ\text{C}$ across the glass transition temperature and then heated back to $T_g+50^\circ\text{C}$. Such experiments were undertaken at 5 modulation periods (60s, 80s, 100s, 120s, and 140s).

Fig. 3 shows the C_p^{real} or in-phase C_p to display a rounded step with the step shifting to higher T as the frequency increases. The $C_p^{imaginary}$ term or out-of phase C_p displays a Gaussian-like peak and the peak steadily shifts to higher T as the modulation frequency increases.

In these scans, the peak location of the $C_p^{imaginary}$ term recorded at 100 sec modulation period defines the glass transition temperature T_g . At the peak location, the relaxation is defined by the condition expressed by $\omega\tau = 1$, where τ is the relaxation time at the peak and ω is the relaxation frequency. Thus, the shift of the peak in $C_p^{imaginary}$ to higher temperatures as the modulation frequency is increased signals a reduction in the melt shear relaxation time. By plotting the variation of $\log_{10}\tau$ against $1/T$ normalized to $1/T_g$, we deduced the fragility index \mathcal{M} using equation (1). Fig 3b illustrates the results for the case of 3 melt compositions of $x = 10\%$, 24% and 27% . The enthalpic activation energy E_a associated with the fragility \mathcal{M} is related to T_g by the following relation:

$$E_a = \mathcal{M}RT_g \ln 10 \quad (3)$$

The compositional variation of the fragility index $\mathcal{M}(x)$ and the activation energy $E_a(x)$ for our $\text{As}_x\text{Se}_{100-x}$ melts of proven homogeneity are displayed in Fig. 4 and 5, respectively. Our

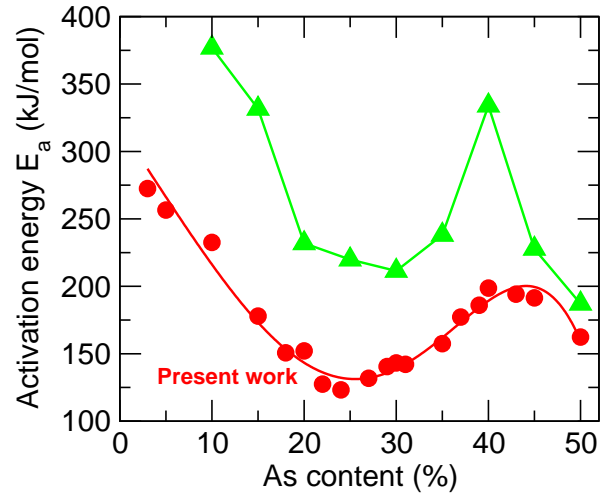


Figure 5: Compositional variation of the activation energy E_a (●, present work), computed from the fragility index (Fig. 4), and compared to previous results from Yang et al. (▲, Ref. 26).

results show both $\mathcal{M}(x)$ and $E_a(x)$ to reveal a broad global minimum centered around $x = 25\%$. Specifically, melt compositions in the $20\% < x < 35\%$ display a fragility index \mathcal{M} of 20 or less. The lowest fragility index (16.4) is obtained for a melt at $x = 24\%$. The melts in this strong region homogenize far more slowly compared to the more fragile melts, most of which homogenize in under 3 days without rocking. This correlation is remarkable, and we comment on it below.

In Fig 4 we have also included fragility results from Viscosity measurements of Musgrave et al.²⁵ and Complex C_p measurements of G. Yang et al.²⁶. There are clear similarities in global trends in all these data as all display a minimum for \mathcal{M} around the 25% As content. The viscosity derived and present mDSC derived fragility index for a melt at $x = 10\%$ are in excellent agreement, although such is not the case at other melt compositions examined. The Complex C_p derived fragility index of Yang et al.²⁶ are of interest because those were obtained the same measuring technique and the same calorimeter as in the present case.

B. Volumetric measurements

Mass density of glassy solids provides useful characterization of a glassy solid. If one inverts it to deduce the molar volume V_m , then one obtains information on network packing. Unlike scanning calorimetric methods and Raman scattering that require a minuscule amount (≈ 20 mgms) of the glass, mass density measurements were made using 200 mgms of a bulk glass to achieve an accuracy of 0.25%. Thus, it is possible to get a global average on a batch preparation and gauge its homogeneity.

We have performed mass density measurements on the bulk $\text{As}_x\text{Se}_{100-x}$ glasses using a quartz fiber and a digital microbalance. A bulk glass specimen typically 200 mgm in size was weighed in air and in 200 Proof Alcohol, and the density ob-

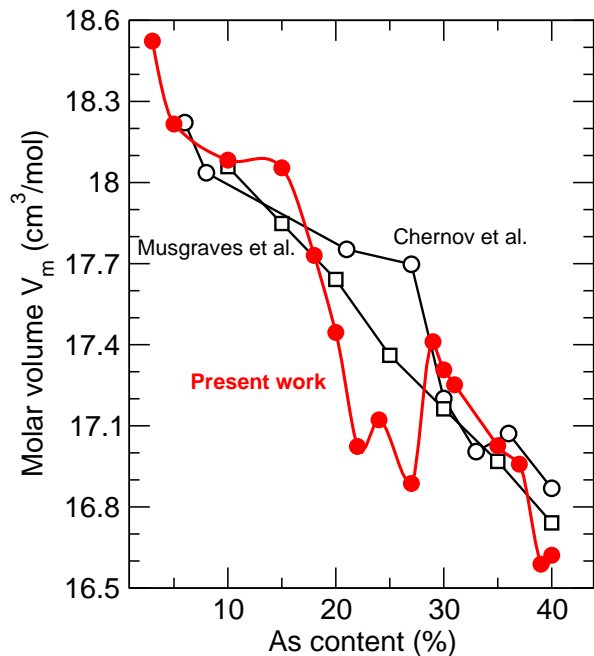


Figure 6: Observed compositional molar volume profile V_m in the As-Se system (●, present work), compared to previous measurements: (□, Ref. 25) and (○, Ref. 29). The large variation in the reported values reflects the differences in melt homogenization in the samples.

tained using Archimedes principle. A single crystal of Si was used to calibrate the density of alcohol and a single crystal of Ge used to check the accuracy of density measurements. In Figure 6 we compare results of molar volume measurements from the present work with several previous reports where complete trends across a wide range of compositions are available.

Several groups report^{25,29,30} an almost linear variation of $V_m(x)$ with x in the $0 < x < 40\%$ range. In our case we observe a variation that departs from linearity particularly in the $20\% < x < 30\%$ range. Nonlinear variation of $V_m(x)$ have been reported for other systems as well³¹ and are related to the stress-free character of the network³². Given that the error in $V_m(x)$ in our measurements is twice the size of the data point, the variance between different group exceeds the error of measurements and is most likely due to sample make up.

IV. DISCUSSION

The present experimental results raise several basic issues on the compositional dependence of physical properties of melts and glasses. In this section we discuss some of these.

A. Fragility index and physics of melt homogenization

We are not aware of any measurement of viscosity in As-Se at the reaction temperature of 700° , and most of the avail-

able experimental data are being found either at much lower temperatures or are restricted to selected compositions^{26,33,34}. Given the compositional trends in $\mathcal{M}(x)$ and the glass transition temperature $T_g(x)$ accessible from the Complex C_p measurements (Figs. 3), we can calculate the variation of the viscosity $\eta(x)$ at 700°C using two seminal models for viscosity variation with temperature. For the VFT, we obtain $\eta(T)$ using :

$$\log_{10} \eta(T) = \log_{10} \eta_\infty + \frac{(12 - \log_{10} \eta_\infty)^2}{\mathcal{M}(T/T_g - 1) + (12 - \log_{10} \eta_\infty)} \quad (4)$$

which is an alternative form of equ. (2), and for the MYEGA equations⁷:

$$\log_{10} \eta(T) = \log_{10} \eta_\infty + (12 - \log_{10} \eta_\infty) \frac{T_g}{T} \times \exp \left[\left(\frac{\mathcal{M}}{12 - \log_{10} \eta_\infty} - 1 \right) (T/T_g - 1) \right] \quad (5)$$

respectively.

It is instructive to consider a model due to Mauro et al. (MYEGA), which gives $\eta(T)$ using equation (5). At high T , and in fragile melts, there is evidence that the MYEGA model works better than the Vogel-Fulcher-Tamman (VFT) model or the Avramov-Milchev model. Using Maxwell's relation $\eta_\infty = G_\infty \tau$ to obtain the viscosity, assuming an infinite frequency shear modulus $G_\infty \simeq 10$ GPa for the As-Se system³⁵, we obtain $\eta(x)$ at the experimental reaction temperature (700°C) for both the VFT and MYEGA equations, and these results are summarized in Figure 7.

A remarkable feature of the plot of Fig. 7 is the six orders of magnitude change in viscosity of $\text{As}_x\text{Se}_{100-x}$ binary melts at 700°C with glass composition. Se-rich ($x < 10\%$) melts are fragile ($\mathcal{M} > 40$) and we note that the viscosity is quite low as it is estimated at 0.05 Pa.s at the target temperature. On the other hand, melts at $x > 24\%$ that are viewed as strong ($\mathcal{M} \simeq 15-20$), the viscosity increases to $\simeq 200$ Pa.s. In correspondence with the strong melts in the fragility index profile, a plateau is observed in the viscosity profiles which suggests that diffusion of the corresponding melts would be inhibited, as evidenced by the delayed homogenization. The delayed diffusion would naturally lead to a density-dependent organization of the vertical melt, leading to the melt fractionation shown, for example, in Figure 2. The high viscosities involved would hinder mixing, even when subject to rapid agitation. These striking increase in melt-viscosity will translate in correspondingly lowering of diffusivity $D(x)$, given that D depends inversely on melt viscosity through e.g. the Eyring relation³⁶.

One thus expects a melt at $x = 24\%$ weighted from an appropriate mix of Se glass ($x=0\%$) and As_2Se_3 glass ($x=40\%$), to rapidly (12 hours) alloy in the initial stages as Se diffuses into the 40% glass and lowers the average stoichiometry to the $15\% < x < 35\%$ range. At this point, the alloying process slows down qualitatively since the strong melts formed now diffuse rather slowly. The decrease (respectively increase) of D (η) by 4 orders of magnitude for melts in the $15\% < x < 35\%$ composition range slows down the melt-mixing and thus

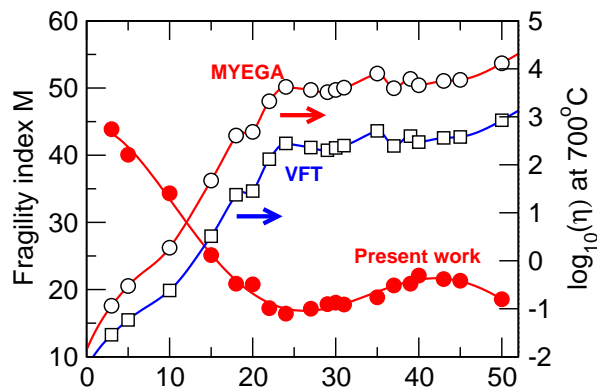


Figure 7: a) Left, fragility index in As-Se melts as a function of As content (same as Fig. 4). Right axis: Computed viscosity profile using the VFT and MYEGA equations at the reaction temperature of 700°C.

homogenization as evidenced by the Raman profile data of Fig. 1 and 2. Since the melt alloying process is largely bottlenecked by diffusive processes, melt-rocking can only play a minor role in homogenization, a situation that has been also evidenced for the case of Ge-Se glasses^{4,37}.

A corollary to this observation is that melts once reacted for longer periods (> 3 days) have progressively lower fragilities, with the lowest ‘true’ fragility measured eventually for the homogenized material. Agitation in a rocking furnace would essentially spread the fragile melts along the melt column without aiding the diffusion process necessary for equilibration at the weighed composition. It then follows that compositions with strong melts exist in a background of fragile melts. Melts at any arbitrary location would then, on average, have a higher fragility. It follows quite naturally that larger quantities of melts (>5 grams) would have a greater quantity of fragile melts, leading to higher fragility indices when measured at any location along the melt column. In other words, a mapping of fragilities along the column of underreacted melts would produce a high average fragility. A perusal of the sample synthesis methods of several groups^{25,26,30} shows that typical sample sizes of 20 grams were reacted at 750°C while rocking for 20 hours. Based on the observations stated above, this length of time is insufficient for homogenizing melts of such large quantities. Since vastly different degrees of homogenization is achieved in the first 48 hours of homogenization, measured physical properties are likely to be a function of the reaction time and would differ with the synthesis times and sample sizes.

B. Calorimetric and fragility anomalies

As highlighted in Figs. 4, 5, and 6, trends in fragility, activation energy, and molar volume exhibit an anomaly with As content for compositions roughly found between 22 and 28% As, which result in a minimum value for \mathcal{M} , E_a and V_m . These findings can be compared to calorimetric measurements that have been performed from a MDSC scan in the

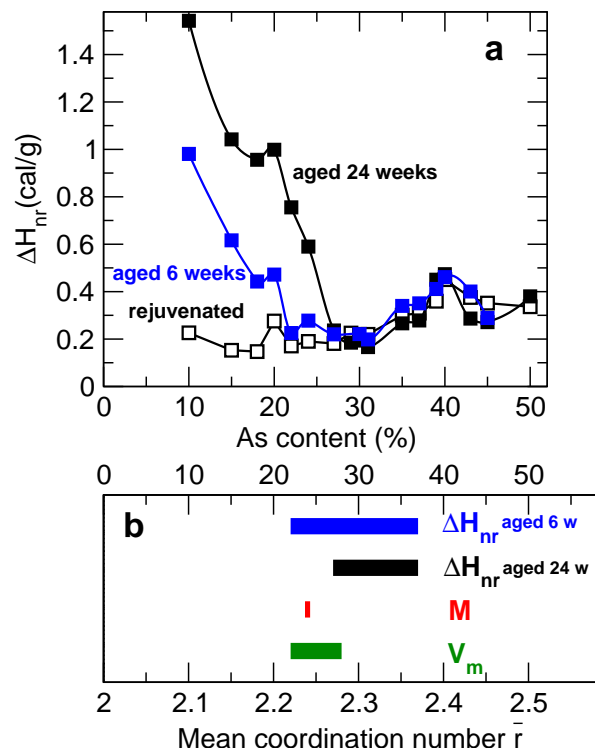


Figure 8: a) Compositional variation of the non-reversing heat flow ΔH_{nr} at the glass transition after six weeks (■), after 24 weeks of ageing at room temperature (■), and after rejuvenation (□). b) Comparison of the different determined compositional windows as a function of As content, and as a function of the mean coordination number \bar{r} .

glass transition region, and which lead to the non-reversing heat flow ΔH_{nr} , a quantity that captures most of the enthalpy of kinetic events associated with the slowing down of the relaxation. Interestingly, ΔH_{nr} displays a minimum as well in As-Se glasses (Fig. 8a, similarly to previous findings²⁴, and to other chalcogenides^{4,15–17,19,20}). The nearly vanishing of ΔH_{nr} which defines a reversibility window, is usually correlated with the existence of an adaptative intermediate phase^{38–40} that is found between the chalcogen-rich flexible phase, and the As-rich stressed rigid phase. The existence the reversibility window is, in fact, a direct consequence of the formation of an isostatic (stress-free) glass network that minimizes both stress (present at high As content) and the floppy modes (present at low As content) which would serve as impetus for relaxation. Without stress and without floppy modes, there is a significantly reduced thermodynamic driving force for relaxation and also a greater kinetic barrier to be overcome to induce relaxation. This direct relationship has been established from a Keating-Kirkwood model¹⁸ showing that for an amorphous solid in which atoms are constrained by a potential containing both the stretching and bending interactions, the enthalpic overshoot in the glass transition endotherm is large for both flexible and stressed rigid networks, but it is minuscule for isostatic networks. It has also been demonstrated from pressure Raman experiments⁴¹ showing that when $\Delta H_{nr} \simeq 0$, networks are stress-free and the Raman lines highly sensitive

to small pressure changes, similarly to the well-known behavior in crystals⁴².

In Fig. 8b, we represent the different compositional windows obtained from the measurements, and it reveals an interesting correlation between the different quantities. The fragility minimum at 24% As is indeed obviously tied to the compositional window found for the molar volume ($22\% < x < 28\%$) and to the reversibility window in ΔH_{nr} for fresh samples ($22\% < x < 37\%$). However, one should note that the exact boundaries can not be fully inferred as for the case of Ge-Se^{4,20}. In particular, the boundaries of the reversibility window are found to evolve with ageing time, especially on the chalcogen-rich side ($x < 22\%$) and lead to a window approximately centred around 30% As after 6 months of ageing.

When represented as a function of the mean coordination number \bar{r} , one obviously finds a slight shift of the location of these anomalies with respect to the mean-field flexible to rigid transition of $\bar{r}=2.4$. It has been suggested that there may be some structural features⁴³ specific to the present As-Se or its sulfide analogue⁴⁴ which increase the isostatic character of the network at lower connectedness²⁴ and bring the onset of rigidity to lower As content. There are at this stage no experimental indication or signatures for such isostatic local structures although numerical evidence has been found in deep supercooled liquids close to the glass transition⁴⁵ and in glasses⁴⁶. However, since all typical features⁴⁷ of flexible, intermediate, and stressed rigid phases are found as the As content is increased, molar volume minima³², reversibility windows¹⁵⁻²⁰, fragility anomaly⁴, one can safely assign the flexible phase to compositions having $x < 20\%$, and the stressed rigid phase to glasses with $x > 37\%$ As. These boundaries actually also agree with recent ab initio simulations showing various structural and dynamic anomalies to occur $\simeq 30\%$ As⁴⁸, in agreement with those found in rigidity transitions driven by pressure^{49,50}.

C. Anomalies in scaling laws

Scaling laws have been widely used for the analysis of relaxation phenomena in supercooled liquids. Here we investigate for the As-Se the validity of a scaling law relating the fragility index to the glass transition temperature. There is indeed a conventional wisdom suggesting that fragility increases with the glass transition temperature¹¹ which implicitly underscores the fact that energy barriers for relaxation increase with increasing T_g .

The derivation of this scaling law uses the definition of equ. (2), and calculates, using equ. (1), the fragility and the activation energy as a function of the glass transition temperature:

$$\mathcal{M} = \frac{AT_g}{(T_g - T_0)^2 \ln 10} \quad (6)$$

and:

$$E_a = \frac{AT_g^2}{(T_g - T_0)^2} \quad (7)$$

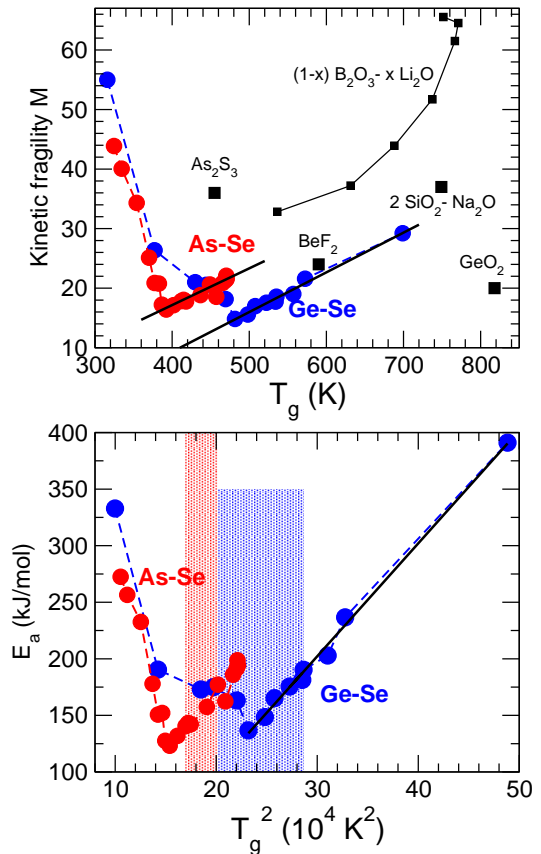


Figure 9: a) Fragility as a function of glass transition temperature in As-Se (red) and Ge-Se liquids (blue, Ref. 4), together with data for typical network glass formers^{23,53,54} and binary glasses⁵⁵. b) Activation energy E_a as a function of T_g^2 . The shaded zones are the corresponding IP₄'s.

As T_g is of the same order as T_0 , one will have \mathcal{M} and E_a which will scale with T_g and T_g^2 , respectively. Note that this can be also independently derived from an alternative form using the Williams-Landel-Ferry (WLF) function for viscosity¹.

Using such scaling laws, Qin and McKenna⁵¹ have shown that the correlations (6)-(7) were fulfilled in a large class of hydrogen bonding organics, polymeric and metallic glass formers as all these systems show a linear increase of \mathcal{M} with T_g , and E_a with T_g^2 . On the other hand, these authors remarked that inorganic glass formers did not seem to follow such scaling laws and \mathcal{M} appeared to be nearly independent of the glass transition temperature. Figure 9 represents the behavior of the fragility index (same as Fig. 4) as a function of the measured glass transition temperature $T_g(x)$ for the present As-Se, together with previous results on Ge-Se⁴. It is found that when off-stoichiometric melts are followed in detail as a function of composition, one recovers the scalings laws (6)-(7) for only selected compositions corresponding merely to the stressed rigid and intermediate phase, i.e. one has a linear increase in $\mathcal{M}(T_g)$ for $x > 22\%$ in Ge-Se⁴, and for $x > 27\%$ in As-Se. A least-square fit to such compositions yields to $\mathcal{M} =$

7.53(5)+0.061(7) T_g and to $\mathcal{M}=-17.356+0.060(1)T_g$ for As-Se and Ge-Se, respectively. The slope of both curves ($\simeq 0.06$) is found to be somewhat lower than the one obtained⁵¹ for metallic glass-formers (0.17), polymers (0.28) and hydrogen bonded liquids (0.25). However, as noted earlier⁵¹, no correlation is found among the various network formers such as B_2O_3 ⁵⁵, GeO_2 ²³ or As_2S_3 ⁵³.

Interestingly, a negative correlation is recovered, as for the case of Ge-Se⁴, which obviously can not be accounted from the VFT equation given that it would lead to unphysical behaviors such as the divergence of relaxation at a temperature $T_0 > T_g$ or an increase of relaxation time τ with temperature⁴. An inspection of the different viscosity models shows that only the VFT equation (2) (or (4)) can lead to a positive correlation (6) between \mathcal{M} and T_g . In fact, a simple Arrhenius behavior yields from equ. (2) $\mathcal{M}=A/T_g \ln 10$ and the MYEGA equation (5) written in its compact form⁷:

$$\log_{10} \eta = \log_{10} \eta_{\infty} + \frac{K}{T} \exp \left[C/T \right] \quad (8)$$

leads to:

$$\mathcal{M} = \frac{K}{T_g} \left(1 + \frac{C}{T_g} \right) \exp \left[C/T_g \right] \quad (9)$$

and for the apparent activation energy:

$$E_a = K \ln 10 \left(1 + \frac{C}{T_g} \right) \exp \left[C/T_g \right] \quad (10)$$

which both decrease as T_g increases.

1. Constraints on the apparent activation energy

Obviously, none of the forms for viscosity (eqs. (2) and (8)) can reproduce the obtained trend in $\mathcal{M}(T_g)$ of Fig. 9. Rather than imagining an alternative form for $\eta(T)$ able to display both positive and negative correlations in $\mathcal{M}(T_g)$, we derive the conditions that should apply at the glass transition on the apparent activation energy $E(T)$ involved in a function describing viscosity (or relaxation or diffusion) with temperature:

$$\log_{10} \eta = \log_{10} \eta_{\infty} + \frac{E(T)}{T} \quad (11)$$

for which the fragility index is given by:

$$\mathcal{M} = \frac{E(T_g)}{T_g} - \left[\frac{dA(T)}{dT} \right]_{T=T_g} = \frac{E(T_g)}{T_g} - E'(T_g) \quad (12)$$

out of which we can calculate the slope:

$$\frac{d\mathcal{M}}{dT_g} = -E''(T_g) + \frac{E'(T_g)}{T_g} - \frac{E(T_g)}{T_g^2} \quad (13)$$

One must thus have for flexible glasses the conditions:

$$E''(T_g) + \frac{E(T_g)}{T_g^2} > \frac{E'(T_g)}{T_g} \quad (14)$$

and:

$$\frac{d^2\mathcal{M}}{dT_g^2} > 0 \quad (15)$$

It is easy to check that either eqs. (2) or (8) only partially fulfill the differential inequalities so that they can not be used for the full trend in $\mathcal{M}(T_g)$ seen in Fig. 9.

2. Competing effects

On a more general ground, it is seen that in order to find such negative correlations in $\mathcal{M}(T_g)$, one must either have an extremum in \mathcal{M} or in T_g , the former situation being found in the present chalcogenides whereas the latter is encountered for e.g., lithium borate glasses (Fig. 9) which show a steady increase of \mathcal{M} with alkali concentration⁵⁵ but a maximum in T_g . Both situations will lead to a branch with a negative slope in a (\mathcal{M}, T_g) plot. Such a situation is not met in other glass-forming liquids where the positive correlation for $\mathcal{M}(T_g)$ holds. By varying the molecular weight and cross-linking density in polymers, several authors⁵⁶⁻⁵⁸ have, indeed, demonstrated that such changes affect \mathcal{M} and T_g in a similar fashion, and an increase in both the fragility and T_g as a function of e.g. the cross-link density.

The physics which drives the trends in $\mathcal{M}(T_g)$ actually results from two independent evolutions $\mathcal{M}(x)$ and $T_g(x)$ with composition, yet related to the underlying structural changes. It has been shown that T_g is an accurate measure of network connectivity⁵⁹⁻⁶¹ and follows very precisely any coordination change induced by chemical alloying. This is not only true for chalcogenides but also for binary oxides such as alkali germanate or borate glasses for which a maximum in T_g is obtained when the population of some higher-coordinated species maximizes with modifier content^{31,55,62}. Ultimately, it is seen that the change from a negative to a positive correlation is strongly tied to the minimum found for the fragility index \mathcal{M} (Fig. 8) and to the reversibility window. Based also on the previous findings on Ge-Se melts⁴, this seems to suggest that flexible chalcogenide glasses will generally display a negative correlation given that they always exhibit an increase of T_g with connectivity but a decrease towards the fragility minimum found in the intermediate phase, whereas stressed rigid glasses will behave the opposite way.

On the other hand, flexible Se-rich supercooled liquids have the same structural morphology as cross-linked polymeric melts for which the VFT or the WLF equations fit quite accurately the viscosity evolution, and which subsequently lead to the reported positive correlation⁵¹ for $\mathcal{M}(T_g)$. Furthermore, the glass transition temperature variation of such flexible As-Se glasses can be quite accurately described⁶³ from the Gibbs-Di Marzio equation⁶⁴ derived for cross-linked polymers. When this category of glass-forming liquids is considered, it is therefore quite unexpected that glasses with a chain-like structure do not follow the positive correlation.

V. CONCLUSION

Melt homogenization is a critical subject that is, unfortunately, often overlooked in the literature. In this article, we have shown that for off-stoichiometric compositions important physical properties crucially depend on the melt processing, and the way melts homogenize at the reaction temperature. For the present case of As-Se liquids, it is found that while compositional trends (i.e. the relative variation) in fragility index \mathcal{M} do not differ with samples having been homogenized over smaller reaction times²⁶, the absolute magnitude of \mathcal{M} is substantially altered with differences up to about a factor two. Carefully homogenized systems over long periods then lead to melts having one of the lowest known fragilities ($\mathcal{M} \simeq 16.4$ for the 24% As glass), lower than the archetypal strong-glass former silica. This allows understanding the origin of the slow homogenization dynamics which arises from the nature of these *super-strong melts* in the range of 25-35% As, having potentially large viscosities, and prevents from fast mixing. Raman profiling confirms the overall tendencies and clearly shows that an important spread in composition still exists along the melt column after 3 days alloying (Fig. 2), a time interval that already exceeds what has been routinely used in earlier studies. These results appear to be generic, and parallel to recent findings on another important chalcogenide system, Ge-Se⁴.

Having obtained glasses and melts of proven homogeneity, we then investigate the effect of As composition on melt fragility. The obtained fragility minimum appears to be directly related to flexible to stressed rigid transitions, and to the reversibility window revealed by the nearly vanishing of the non-reversing heat flow ΔH_{nr} . It is also found that homogenization impacts glass network packing such as molar volumes which display a minimum for the same compositions, a feature that originates from the stress-free nature of the network backbone. In this respect, the present As-Se reproduces all the well-established features of isostatic windows such as space-filling tendencies³², thermally-reversing character of the glass transition¹⁷, and fragility anomalies⁴.

Given the reported impact of glass sample make up^{19,20} on physical properties of network glasses, the crucial role played by melt homogenization and glass processing should once again be emphasized at the end. Based on the present work, and on the previous example of Ge-Se⁴, we are convinced that glasses of proven homogeneity will certainly exhibit the intrinsic behavior of adaptive networks undergoing a flexible to rigid transition over a finite width of stress-free compositions.

PB acknowledges support from NSF grant DMR-08-53957. MM acknowledges support from ANR grand 09-BLAN-0109-01, from the Franco-American Fulbright Commission and from International Materials Institute.

-
- ¹ J.D. Ferry, *Viscoelastic Properties of Polymers*, (Wiley, New York, NY, 1980).
 - ² D. Huang, G. McKenna, *J. Chem. Phys.* **114**, 5621 (2001).
 - ³ S.L. Simon, D.J. Plazek, J.W. Sobieski, E.T. McGregor, *J. Polym. Sci. B* **35**, 929 (1997).
 - ⁴ K. Gunasekera, S. Bhosle, P. Boolchand, M. Micoulaut, *J. Chem. Phys.* **139**, 164511 (2013).
 - ⁵ A. Kushima, X. Lin, J. Li, J. Eapen, J.C. Mauro, X. Qian, P. Diep, S. Yip, *J. Chem. Phys.* **130**, 224504 (2009).
 - ⁶ H. Vogel, *Phys. Z.* **22**, 645 (1921); G. Tamman, W. Hesse, *Z. Anorg. All. Chem.* **156**, 245 (1926); G.S. Fulcher, *J. Am. Ceram. Soc.* **8**, 339 (1925).
 - ⁷ J.C. Mauro, Y. Yue, A.J. Ellison, P.K. Gupta, D.C. Allan, *Proc. Nat. Acad. USA* **106**, 19780 (2009).
 - ⁸ I. Avramov, A. Milchev, *J. Non-Cryst. Solids* **104**, 253 (1988).
 - ⁹ Q. Qin, G. McKenna, *J. Non-Cryst. Solids* **352**, 2977 (2006).
 - ¹⁰ W.T. Laughlin, D.R. Uhlmann, *J. Phys. Chem.* **76**, 2317 (1972).
 - ¹¹ C.A. Angell, *Science* **67**, 1924 (1995).
 - ¹² M. Tatsumisago, B.L. Halfpap, J.L. Green, S.M. Lindsay, C.A. Angell, *Phys. Rev. Lett.* **64**, 1549 (1990).
 - ¹³ J.C. Phillips, *J. Non-Cryst. Solids* **34**, 153 (1979).
 - ¹⁴ M.F. Thorpe, *J. Non-Cryst. Solids* **57**, 355 (1983).
 - ¹⁵ D. Selvenathan, W. Bresser, P. Boolchand, *Solid State Commun.* **111**, 619 (1999).
 - ¹⁶ F. Wang, S. Mamedov, P. Boolchand, B. Goodman, M. Chandrasekhar, *Phys. Rev. B* **71**, 174201 (2005).
 - ¹⁷ S. Bhosle, P. Boolchand, M. Micoulaut, C. Massobrio, *Solid State Comm.* **151**, 1851 (2011).
 - ¹⁸ M. Micoulaut, *J. Phys. Cond. Matt.* **22**, 285101 (2010).
 - ¹⁹ S. Bhosle, K. Gunasekera, P. Boolchand, M. Micoulaut, *Int. J. Appl. Glass Science* **3**, 205 (2012).
 - ²⁰ S. Bhosle, K. Gunasekera, P. Boolchand, M. Micoulaut, *Int. J. Appl. Glass Science* **3**, 189 (2012).
 - ²¹ T. Scopigno, G. Ruocco, F. Sette, G. Monaco, *Science* **302**, 849 (2003).
 - ²² V.N. Novikov, Y. Ding, A.P. Sokolov, *Phys. Rev. E* **71**, 061501 (2005).
 - ²³ R. Böhmer, K. L. Ngai, C. A. Angell, and D. J. Plazek, *J. Chem. Phys.* **99**, 4201 (1999).
 - ²⁴ D. G. Georgiev, P. Boolchand, M. Micoulaut, *Phys. Rev. B* **62**, R9228 (2000).
 - ²⁵ J. D. Musgraves, P. Wachtel, S. Novak, J. Wilkinson, K. Richardson, *J. Appl. Phys.* **110**, 063503 (2011).
 - ²⁶ G. Yang, O. Gulbiten, Y. Gueguen, B. Bureau, J.-Ch. Sangleboeuf, C. Roiland, E.A. King, and P. Lucas, *Phys. Rev. B* **85**, 144107 (2012).
 - ²⁷ S.A. Degretov, A.D. Pelton, and J.D. L'Ecuyer, *J. Phase Equilibria* **18**, 357 (1997).
 - ²⁸ H. Okamoto, *J. Phase Equilibria* **19**, 488 (1998).
 - ²⁹ A. P. Chernov, S. A. Dembovskii, and S. F. Chistov, *Izv. Akad. Nauk SSSR, Neorg. Mater.* **4**, 1658 (1968).
 - ³⁰ A Feltz, H Aust, A Blayer, *J. Non-Cryst. Solids* **55**, 179 (1983).
 - ³¹ R. Rompicharla, D.I. Novita, P. Chen, P. Boolchand, M. Micoulaut, W. Huff, *J. of Phys. Cond. Matt.* **20**, 202101 (2008).
 - ³² C. Bourgel, M. Micoulaut, M. Malki, P. Simon, *Phys. Rev. B* **79**, 024201 (2009).
 - ³³ J. Mälek, J. Šhanelová, *J. Non-Cryst. Solids* **351**, 3458 (2005).
 - ³⁴ G. Yang, T. Rouxel, J. Troles, B. Bureau, C. Boussard-Plédel, P. Houizot, J.-C. Sangleboeuf, *J. Am. Ceram. Soc.* **94**, 2408 (2011).
 - ³⁵ Z.U. Borisova, *Glassy semiconductors*, Springer (1981).
 - ³⁶ M. Bauchy, B. Guillot, M. Micoulaut, N. Sator, *Chem. Geol.* **346**, 47 (2013).

- ³⁷ R. Bhageria, K. Gunasekera, P. Boolchand, M. Micoulaut, condmat arXiv:1310.0663.
- ³⁸ M.V. Chubynsky, M.A. Brière, N. Mousseau, Phys. Rev. E **74**, 016116 (2006).
- ³⁹ M. Micoulaut, Phys. Rev. B **74**, 184208 (2006).
- ⁴⁰ J. Barré, A.R. Bishop, T. Lookman, A. Saxena, Phys. Rev. Lett. **94**, 208701 (2005).
- ⁴¹ F. Wang, S. Mamedov, P. Boolchand, B. Goodman, M. Chandrasekhar, Phys. Rev. B **71**, 174201 (2005).
- ⁴² C.P. Ostertag, L.H. Robins, and L.P. Cook, J. Eur. Ceram. Soc. **7**, 109 (1991).
- ⁴³ T. Wagner, S.O. Kasap, Philos. Mag. B **74**, 667 (1996).
- ⁴⁴ E. Diemann, Rev. Chim. Miner. **16**, 237 (1979).
- ⁴⁵ M. Bauchy, M. Micoulaut, J. Non-Cryst. Solids **377**, 34 (2013).
- ⁴⁶ S. Hosokawa, A. Koura, J.-F. Bérar, W.-C. Pilgrim, S. Kohara, and F. Shimojo, Europhys. Lett. **102**, 66008 (2013).
- ⁴⁷ *Rigidity and Boolchand Intermediate Phases in Nanomaterials*, edited by M. Micoulaut and M. Popescu (INOE Publishing House, Bucarest, 2009). This book is a compilation of a series of chapters written by investigators active in the field of self-organization effects in network glasses.
- ⁴⁸ M. Bauchy, M. Micoulaut, M. Boero, C. Massobrio, Phys. Rev. Lett. **110**, 165501 (2013).
- ⁴⁹ M. Bauchy, M. Micoulaut, Phys. Rev. Lett. **110**, 095501 (2013).
- ⁵⁰ M. Micoulaut, M. Bauchy, Phys. Status Solidi B **250**, 976 (2013).
- ⁵¹ Q. Qin, G.B. McKenna, J. Non-Cryst. Solids **352**, 2977 (2006).
- ⁵² B. O. Mysen and P. Richet, *Silicate Glasses and Melts: Structure and Properties* (Springer, Berlin, 2005).
- ⁵³ G. Ruocco, F. Sciortino, F. Zamponi, C. De Michele, T. Scopigno, J. Chem. Phys. **120**, 10666 (2004).
- ⁵⁴ D. Huang, G.B. McKenna, J. Chem. Phys. **114**, 5621 (2001).
- ⁵⁵ G.D. Chryssikos, E.I. Kamitsos, Y.D. Yiannopoulos, J. Non-Cryst. Solids **196**, 244 (1996).
- ⁵⁶ C.M. Roland, P.G. Santangelo, K.L. Ngai, J. Chem. Phys. **111**, 5593 (1999).
- ⁵⁷ A.K. Rizo, K.L. Ngai, Macromolecules **31**, 6217 (1998).
- ⁵⁸ P.G. Santangelo, C.M. Roland, Macromolecules **29**, 5747 (1996).
- ⁵⁹ M. Micoulaut, G.G. Naumis, Europhys. Lett. **47**, 568 (1999).
- ⁶⁰ M. Micoulaut, Eur. Phys. J. B **1**, 277 (1998).
- ⁶¹ P. Boolchand, D.G. Georgiev, T. Qu, F. Wang, L. Cai, S. Chakravarty, Comptes Rendus Chimie **5**, 713 (2002).
- ⁶² J.C. Mauro, P.K. Gupta, and R.J. Loucks, J. Chem. Phys. **130**, 234503 (2009).
- ⁶³ M. Micoulaut, G.G. Naumis, Europhys. Lett. **47**, 568 (1999).
- ⁶⁴ J.H. Gibbs, E.A. Di Marzio, J. Chem. Phys. **28**, 373 (1958).